Quantum Anomalous Hall Effect in
Perfectly Compensated Collinear Antiferromagnetic Thin Films

Chao Lei,[1] Olle Heinonen,[2] R. J. McQueeney,[3, 4] and A. H. MacDonald[1]

[1]*Department of Physics, The University of Texas at Austin, Austin, TX 78712*
[2]*Materials Science Division, Argonne National Laboratory, Lemont, IL 60439, USA*
[3]*Ames Laboratory, Ames, IA, 50011, USA*
[4]*Department of Physics and Astronomy, Iowa State University, Ames, IA, 50011, USA*
(Dated: October 5, 2021)

We show that the quantum anomalous Hall effect almost always occurs in magnetic topological insulator thin films whenever the top and bottom surface layer magnetizations are parallel, independent of the interior layer magnetization configuration. Using this criteria we identify structures that have a quantum anomalous Hall effect even though they have collinear magnetic structures with no net magnetization, and discuss strategies for realizing these interesting magnetic states experimentally.

Introduction— The anomalous Hall effect (AHE) was observed [1, 2] already in the 19th century, but understood quantitatively only recently [3]. The discovery of the quantum Hall effect [4, 5], and its interpretation [6] in terms of momentum space Chern numbers, played a role in improving understanding of the AHE by clarifying why the intrinsic momentum-space Berry curvature contribution [7], which had sometimes been controversial, can play an important role. For many classes of materials predictive theories of the AHE, including extrinsic skew [8, 9] and side-jump [10] effects along with intrinsic contributions [7], are now available. The theory of the AHE is especially simple in quasi-two-dimensional magnetic insulators, since it is then purely intrinsic and must be quantized.

Historically, the AHE has often been assumed to be proportional to the magnetization, and therefore to be a characteristic of ferromagnets - not antiferromagnets. Indeed, rigorous symmetry arguments can be used to rule out an AHE in antiferromagnets with a combined $\mathcal{TO}$ symmetry, where $\mathcal{T}$ is time reversal and $\mathcal{O}$ is any unitary symmetry operator - for example a lattice translation operator. This argument rules out an anomalous Hall effect in the common collinear antiferromagnets of bipartite crystals. However, AHEs do occur in both non-collinear [11–17] and collinear [18, 19] antiferromagnets that do not possess a symmetry of this type. AHEs in antiferromagnets are of technological interest because they provide easy access to information stored in hysteretic antiferromagnetic order configurations.

The property that the Hall conductivity of any two-dimensional crystal $\sigma_{xy} = \sigma e^2/h$ is quantized was recognized [20] as an outgrowth of the topological theory [6] of the quantum Hall effect [4]. Non-zero integer values of σ can be produced not-only by external magnetic fields but also, in the case of the quantized anomalous Hall effect (QAHE), by spontaneous time-reversal symmetry breaking. The QAHE was first realized [21] experimentally, in work motivated by a theoretical proposal [22], in magnetically doped and ferromagnetically ordered topological insulators. The possibility of a QAHE in non-collinear,

and non-coplanar two-dimensional antiferromagnets has been thoroughly explored theoretically [23–27]. Here we predict that the QAHE also occurs in magnetic topological insulator (MTI) thin films with perfectly compensated collinear magnetic order when the top and bottom surface layer magnetizations are parallel, and discuss how these magnetic configurations can be realized experimentally.
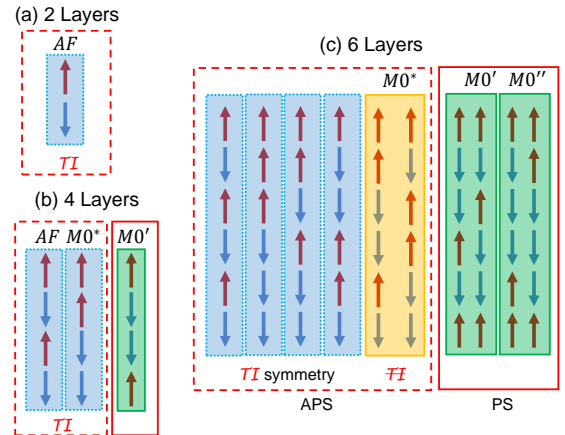

FIG. 1. Fully compensated magnetic configurations of 2, 4, and 6 layer MTI thin films. Only configurations that are distinct under global spin reversal are illustrated. Odd parity configurations (blue) yield a band Hamiltonian with $\mathcal{TI}$ symmetry and necessarily have Hall quantum integer $\sigma = 0$. We find that configurations that are not odd parity, but still have anti-parallel surface layers (APS) (orange) almost always have $\sigma = 0$, while those with parallel surface layers (PS - green) almost always have $\sigma \neq 0$.

Qualitative QAHE Criteria— $\mathrm{Mn(Sb}_x\mathrm{Bi}_{1-x})\mathrm{X}_4$ thin films consist of van der Waals coupled septuple layers with ferromagnetically ordered Mn local moments at their centers, and perpendicular-to-plane easy axes [28–32]. The ferromagnetic layers are coupled via weak antiferromagnetic exchange interactions that act across the van der Waals gap. This interesting family of materials has recently attracted both theoretical and experi-

mental interest [28–62]. Compensated antiferromagnetic states with equal numbers of ↑ and ↓ layers are possible for even layer number N. The number of compensated magnetic configurations is $C(N, N/2) = 2, 6, 20 \ldots$ for $N = 2, 4, 6 \ldots$. Each of these combinations has a time-reversed partner whose Chern number differs by a sign. Choosing one member from each time-reversed pair leaves the $C(N, N/2)/2$ configurations, illustrated for $N = 2, 4, 6$ in Fig. 1, to be studied.

Our analysis of MTI thin films is based on a simplified couple Dirac cone model [33] applicable to the $Mn(Sb_xBi_{1-x})X_4$ X = (Se,Te) family of intrinsic magnetic topological insulators (IMTIs), QAHEs are expected to be common in odd N uncompensated films, and have been observed in MBT ($MnBi_2Te_4$) thin film with $N = 5$ [44]. QAHEs have also been observed at other film thicknesses [42, 44, 51] when the magnetic configurations is altered by applying magnetic fields larger than ≈ 5 T. In Fig. 1 we classify the magnetic configurations of even N compensated moment MTI thin films as either antiparallel surface layer (APS) or parallel surface layer (PS), depending on whether the magnetizations of the top and bottom surface layers are anti-parallel or parallel. For large even N the number of PS configurations is almost equal to the number of APS configurations [63]. Many APS films have odd-parity magnetization configurations in the sense that their magnetizations are reversed when the layer order is reversed. The mean-field Hamiltonians of this subset of APS films (blue in Fig. 1) can be shown [64] to have $\mathcal{TI}$ symmetry and hence $\sigma = 0$. We find numerically that even APS films that do not have this symmetry (orange in Fig. 1) almost always have $\sigma = 0$. On the other hand PS magnetic configurations (green in Fig. 1) often have $\sigma \neq 0$, even though their moments are perfectly compensated.

We start by examining the $N = 2$, $N = 4$ and $N = 6$ cases in detail. $C(N, N/2)/2 = 1$ for $N = 2$, leaving one configuration to be studied. Since this configuration has odd parity, the mean-field Hamiltonian has $\mathcal{TI}$ symmetry and we know without calculation that Berry curvature vanishes and $\sigma = 0$. The thinnest PS configuration occurs at $N = 4$. The 3 configurations of $N = 4$ thin film in Fig. 1(b) are labelled AF, $M0^*$ and $M0'$. Among these only the MO' (↑↓↓↑) state has PS configuration and thus can host a QAHE state. For $N = 6$, four of the ten illustrated configurations have $\mathcal{TI}$ symmetry and thus zero Berry curvature and $\sigma = 0$. To determine whether or not the two remaining APS magnetic configurations (denoted as $M0^*$) and the four PS configurations (denoted as $M0'$ and $M0$") in Fig. 1 (c)) support QAHE states, it is necessary to examine the electronic structure more closely.

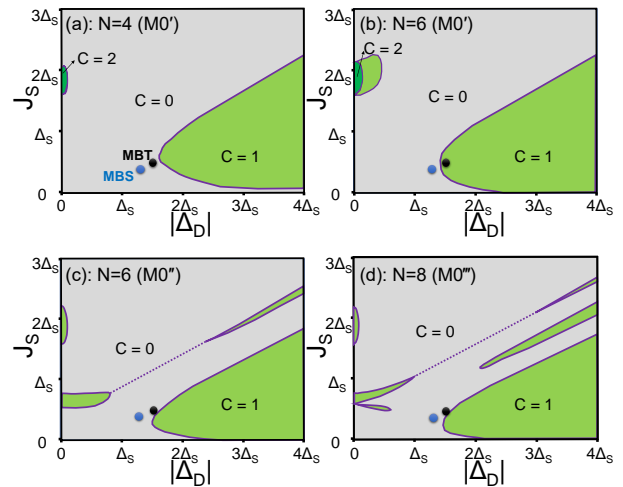*Model Calculations*— We employ a low-energy phenomenological band model, discussed in detail in [33],

FIG. 2. MTI thin film phase diagrams for a variety of fully compensated PS magnetic configurations. The x and y axes are the ratio of the interlayer to intralayer hybridization $|\Delta_D|/\Delta_S$ and the ratio of exchange and hybridization parameters J_S/Δ_S. The phase boundary is also sensitive to $\delta \equiv J_D/J_S$, the ratio of the exchange coupling to adjacent layer moments to the exchange coupling to same layer moments, which is fixed in these plots at $\delta = 0.8$, the value estimated for MBT. Phase diagrams for larger and smaller values of δ are included in the supplementary material [63]. (a) $N = 4$ M0$'$ state; (b) $N = 6$ M0$'$ and (c) $N = 6$ M0$''$ state; (d) $N = 8$ M0$'''$ state with magnetic configuration (↑↓↓↓↓↑↑↑); The light green regions of the phase diagram have Chern number magnitude $|C| = 1$, whereas the dark green regions have $|C| = 2$ and the grey regions $C = 0$. Model parameters estimated for $MnBi_2Se_4$ and $MnBi_2Te_4$ at temperature $T = 0$ are marked by blue and black dots respectively.

with Dirac cones on both surfaces of each septuple layer:

$$H = \sum_{\mathbf{k}_\perp, ij} \left[\left((-)^i \hbar v_D (\hat{z} \times \sigma) \cdot \mathbf{k}_\perp + m_i \sigma_z \right) \delta_{ij} + \Delta_{ij} (1 - \delta_{ij}) \right] c_{\mathbf{k}_\perp i}^\dagger c_{\mathbf{k}_\perp j}.$$

Here i and j are Dirac cone labels with even integers reserved for septuple layer bottoms and odd for layer tops, $\hbar$ is the reduced Planck constant, v_D is the velocity of the Dirac cones, and Δ_{ij} is the hopping amplitude between the ith j^{th} Dirac cones. Only the four largest model parameters, estimated by fitting to DFT calculations, are retained in our calculations: hopping between the surface Dirac cones in the same layer(Δ_S), nearest neighbour hopping between adjacent layers (Δ_D), and two exchange coupling parameters. The exchange coupling parameter $m_i \equiv \sum_\alpha J_{i\alpha} M_\alpha$ where α is a layer label and $M_\alpha = \pm 1$ specifies the sense of magnetization on layer α. We retain exchange coupling J_S to the magnetization in the same septuple layer and near-neighbor exchange coupling J_D to the magnetism in the adjacent septuple layer.

Fig. 2 contains two-dimensional $|\Delta_D|/\Delta_S$-J_S/Δ_S

topological phase diagrams calculated with $\delta \equiv J_D/J_S = 0.8$ - its MBT value [33]. This figure includes phase diagrams for several fully compensated PS magnetic configurations: 4-layer $M0'$, 6-layer $M0'$ and $M0''$, and 8-layer $M0'''$. In the phase diagrams light green regions represent quantum anomalous Hall states with Chern number $C = 1$, the dark green regions represent $C = 2$, and the gray regions represent normal insulators. Quantum anomalous Hall (QAH) states are common in the bottom right regions of these phase diagrams, where Δ_D is large enough to yield TI states in the absence of magnetism and J_S is small enough that the exchange fields perturb the non-magnetic TI state weakly. The model parameters estimated for MBT are close to the phase boundaries between QAH and trivial states because the exchange interactions are relatively weak and because these materials are barely topological in the sense [33] that $|\Delta_D/\Delta_S|$ is not much larger than one.

It is instructive to examine the $J_S = 0$ and $\Delta_D = 0$ lines in the phase diagrams more closely. We do this in Fig. 3 by plotting thin film energy gaps $vs.$ Δ_D at $J_S = 0$ and $vs.$ J_S at $\Delta_D=0$. In Fig. 3 (a) we see that large values of Δ_D increasingly isolate the top and bottom surface Dirac cones and decrease the amplitude for tunneling between them across the bulk of the film. The surface isolation property at large Δ_D can be understood qualitatively by examining the bilayer limit of the Dirac cone model, for which the band gap at $J_S = 0$ is $E_g = \sqrt{\Delta_D^2 + 4\Delta_S^2} - |\Delta_D|$, which goes to 0 whenever $\Delta_D \to \infty$. This property explains the proximity of the QAH region to the $J_S = 0$ line at large $|\Delta_D|$, since very weak exchange is then sufficient to induce a level crossing between the surface states.

Along the $\Delta_D = 0$ line, whose gaps are plotted Fig. 3 (b), each septuple layer is an isolated two-Dirac-cone two-dimensional electron system that contributes a quantum unit to the anomalous Hall effect when its exchange coupling strength exceeds Δ_S. The isolated septuple layer Hamiltonian is

$$H_{SL} = \begin{pmatrix} m_t & v_D k_- & \Delta_S & 0 \\ v_D k+ & -m_t & 0 & \Delta_S \\ \Delta_S & 0 & m_b & -v_D k_- \\ 0 & \Delta_S & -v_D k+ & -m_b \end{pmatrix}, \quad (2)$$

where $k_\pm \equiv k_y \pm ik_x$, and $m_{t/b}$ are top and bottom surface Dirac masses. On the outside surfaces $m_{t/b}$ equals $\pm J_S$, whereas on the interior surfaces $m_{t/b}$ can equal $\pm(J_S + J_D)$ or $\pm(J_S - J_D)$ depending on the magnetic configuration. The eigenvalues of this Hamiltonian are

$$E = \pm \frac{1}{2}\sqrt{4v_D^2|k|^2 + \left(m_+ \pm \sqrt{m_-^2 + 4\Delta_S^2}\right)^2}, \quad (3)$$

where $|k| = \sqrt{k_x^2 + k_y^2}$ and $m_\pm \equiv m_t \pm m_b$. From Eq. 3 we see that the gaps are determined by the band energies at the two dimensional Γ point. Using Eq. 3 it is easy to determine the Hall conductance contributed by each septuple layer along the $\Delta_D = 0$ line in any magnetic

configuration. The $C = 2$ regions along the $\Delta_D = 0$ line in Fig. 2 appear when the surface septuple layers have entered QAH states, but the interior septuple layers still have zero Chern number.
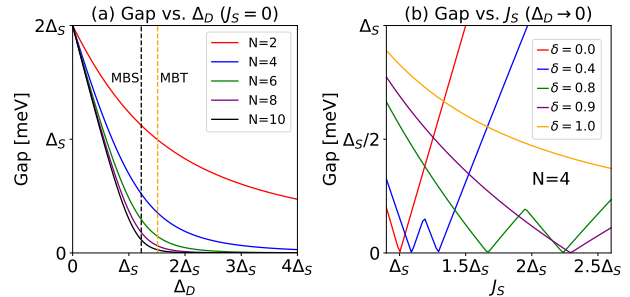

FIG. 3. Gaps $vs.$ hybridization between different septuple layers Δ_D and exchange splitting J_S. The quantized Hall conductance can change value only when gaps close. (a) dependence on Δ_D at $J_S = 0$ for several thin films thicknesses. (b) dependence on J_S at $\Delta_D = 0$ for the four-layer thin film with the parallel surface magnetic configuration. Several different values of $\delta \equiv J_D/J_S$ are considered. For $\delta = 0$ and $\delta = 1$ no topological phase transition occurs as a function of J_S, in the former case because each septuple layer contributes the same sign of Hall conductivity as its spin magnetization, and in the latter case because topological transitions are absent. For other values of δ topological phase transitions occur between $C = 0$ and $C = 2$ states.

The sensitivity of the phase diagram to δ is greatest at small Δ_D. When δ and Δ_D both vanish each septuple layer is driven into a QAH state when $J_S > \Delta_S$ with the Chern number sign depending on the direction of magnetic moment in that layer. It follows that for all perfectly compensated configurations the total Chern number vanishes in this limit. When $\delta \to 1$ on the other hand a variety of different cases must be distinguished. Consider, for example, the top septuple layer when it is isolated by setting $\Delta_D \to 0$. For a $\uparrow\uparrow \cdots$ configurations the energies at Γ are $E = (\pm J_S \pm \sqrt{J_S^2 + 4\Delta_S^2})/2$, whereas for a $\uparrow\downarrow \cdots$ configurations $E = (\pm 3J_S \pm \sqrt{J_S^2 + 4\Delta_S^2})/2$. Similarly for an interior layers with an $\cdots \uparrow\uparrow\downarrow \cdots$ configuration $E = \pm J_S \pm \sqrt{J_S^2 + \Delta_S^2}$, whereas for $\cdots \uparrow\uparrow\uparrow \cdots$ configurations $E = \pm 2J_S \pm \Delta_S$. When level crossings occur as a function of J_S, the isolated septuple layer's contribution to the Hall conductivity changes from 0 to 1. The appearance or absence of QAH phases is easily determined by adding the contributions of all layers. These types of considerations explain the phase transition points along $\Delta_D = 0$ lines in Fig. 2, Fig. 3(b), and in Fig. S5 of the supplemental material[63] which presents phase diagrams for $\delta = 0$ and $\delta = 1$.

$Discussion$— We have shown that magnetic configurations of $\mathrm{Mn(Bi_xSb_{1-x})_2X_4}$ multilayer MTI thin films with parallel magnetizations on surface septuple layers can have QAHEs even though they have perfectly compensated collinear spin moments. The thinnest example is a four layer structure with interior and exterior
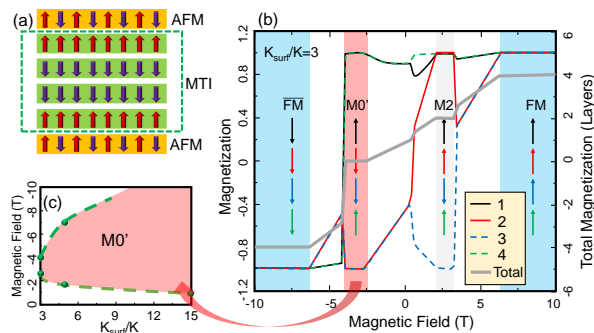
FIG. 4. The $N = 4$ parallel-surface-layer (PS) fully compensated collinear magnetic configurations can be realized by reversing the orientations of the top or bottom layers relative to the interior layers using exchange bias. The red and purple arrows in (a) represent moment orientations. (b) shows the $z-direction$ total magnetization that is predicted by classical Monte Carlo simulation of a $N = 4$ film at the temperature of 0.1 K. The effective surface layer magnetic anisotropy is 3 time the interior layer magnetic anisotropy. The shaded regions have collinear magnetic configurations, and the integer portion of the configuration label is the net number of aligned layers. The PS configuration is labelled M0′. (c) shows parameter range of surface magnetic anisotropy and magnetic field over which $N = 4$ PS states occur when the magnetization is swept toward negative values starting from $B = 10$ T.

layer magnetizations having opposite orientations ($\uparrow\downarrow\downarrow\uparrow$), but many more configurations in this category appear in thicker films [63]. The appearance or absence of a QAHE is dependent on the details of electronic structure and magnetic interactions, and that dependence is described here in terms of the parameters of a simplified Dirac-cone model of the electronic structure with hybridization and exchange parameters Δ_S, Δ_D, J_S and J_D that predicts the phase diagrams in Fig. 2. It is possible to some extent to move through this phase diagram experimentally by varying the choice of chalcogen X or the pnictide fraction x in $\text{Mn}(\text{Bi}_x\text{Sb}_{1-x})_2\text{X}_4$, by apply vertical strains, or by increasing temperature to reduce exchange interaction strengths. For the case of MBT with $N \geq 6$ and the chosen parameters, all configurations with parallel surface (PS) layer magnetization have a QAH phase over a finite interval of temperature when thermal fluctuations in local moment orientations are assumed to decrease exchange interaction strengths ($m_i \to \xi m_i$ with $\xi \in (0, 1)$) as shown in Fig. S4 in the supplemental material [63]. For magnetic configurations with anti-parallel surface magnetizations, no gap closings occur as a function of ξ, indicating that all remain in their $\xi = 0$ topologically trivial states (with zero Chern number) at any temperature.

The set of magnetic configurations that can be realized by cycling magnetic field is dependent on magnetic anisotropy. The PS configurations of interest here are accessible when the magnetic anisotropy energy is favorable, either naturally or as a consequence of intentional

interface engineering. For example, in a previous publication [64] we showed that the $N = 6$ PS magnetic configuration M0' state in Fig. 1 (referred to there as M0*) can be reached from the M2′ state when the ratio of the single-ion anisotropy coefficient D to the interlayer exchange interactions J is sufficiently large. Specifically D/zJ must be greater than 0.23, much larger than the D/zJ ratio of bulk MnB_2X_4 which is approximately 0.13. (The bulk single-ion anisotropy energy of MnB_2X_4 $K \equiv DS^2$, where $S = 5/2$, is approximately 0.17 meV and corresponds to a value of $SD = 0.07$ meV. The interlayer exchange interaction $SJ = 0.088$ meV and the interlayer coordination number $z = 6$.) Although it seems likely, therefore, that the bulk anisotropy energy is insufficient to reach PS configurations in MnB_2X_4, it will nevertheless be interesting to explore other materials with similar structures that could very well have more favorable D/zJ ratios, possibly MnBi_4Te_7 where the interlayer coupling strength is much weaker.

Another strategy that can be used to realize PS magnetic configurations is to engineer the effective anisotropy of the surface layers. This could potentially be accomplished by exchange-biasing the surface layers, as illustrated in Fig. 4 (a). Exchange biasing may not be possible for the bottom surface if the choice of substrate is very important for the epitaxial growth of MBT thin films. However, since MBT can be exfoliated, it is possible to transfer exfoliated flakes onto some other insulating AFM such as the (111) surface of FeO in which the magnetization in each (111) plane is perpendicular to the (111) plane. There is more flexibility in engineering the top surface anisotropy since we may grow an insulating AFM with decent coupling on the top surface. Perpendicular exchange bias would provide an added effective uni-directional anisotropy to the surface layers so that the interior layers will switch in an applied magnetic field while the surface layers do not. This qualitative idea is quantified in Fig. 4 (b), which plots the $\hat{z}$-component of total magnetization as a function of magnetic field, as the magnetic field is reversed from a saturating $B = 10$ Tesla field. For the illustrated case in which the surface layer anisotropy is three times the interior layer anisotropy (assumed to equal the bulk crystal value) the PS Chern insulator configuration is stable over a finite range of magnetic field. It is interesting that the magnetic-field cycling strategy can work even though a QAH state with vanishing total spin magnetization. As illustrated in Fig. 4 (c), the Chern insulator configuration with perfect spin moment compensation occurs over a wider and wider range of magnetic field as the surface layer magnetic anisotropy gets stronger and stronger. In principle it is possible to set the exchange bias by applying a large field near the Néel temperature of the insulating AFM and then cool down in field to well below the insulating AFM Néel temperature (below the so-called blocking temperature for exchange bias). For many exchange bias systems, the blocking temperature is much higher than the Neel temperature of MBT. Therefore, in

the relevant temperature range here, the exchange bias on the top and bottom surfaces will then be basically independent of temperature. In this way we can tune the interlayer exchange coupling by tuning the temperature in a regime where the exchange bias remains fixed. PS QAH states are likely easier to realize in thicker films, where conifgurations with this property are abundant, but the QAH effect itself is more vulnerable [65] to unintended external electric fields.

In summary we have shown that MBT thin films have a QAHE in spite of having perfect spin-moment compensation, possibly supported in some metastable magnetic configurations. Magnetic states with these unusual properties could potentially be valuable for applications, if they could be realized in well controlled materials with room temperature magnetic ordering temperatures.

I. ACKNOWLEDGEMENTS

[1] E. Hall, American Journal of Mathematics **2**, 287 (1879).

[2] E. H. Hall, The London, Edinburgh, and Dublin Philosophical Magazine and Journal of Science **12**, 157 (1881).

[3] N. Nagaosa, J. Sinova, S. Onoda, A. H. MacDonald, and N. P. Ong, Rev. Mod. Phys. **82**, 1539 (2010).

[4] K. v. Klitzing, G. Dorda, and M. Pepper, Phys. Rev. Lett. **45**, 494 (1980).

[5] K. von Klitzing, Rev. Mod. Phys. **58**, 519 (1986).

[6] D. J. Thouless, M. Kohmoto, M. P. Nightingale, and M. den Nijs, Phys. Rev. Lett. **49**, 405 (1982).

[7] R. Karplus and J. M. Luttinger, Phys. Rev. **95**, 1154 (1954).

[8] J. Smit, Physica **21**, 877 (1955).

[9] J. Smit, Physica **24**, 39 (1958).

[10] L. Berger, Physical Review B **2**, 4559 (1970).

[11] H. Chen, Q. Niu, and A. H. MacDonald, Phys. Rev. Lett. **112**, 017205 (2014).

[12] S. Nakatsuji, N. Kiyohara, and T. Higo, Nature **527**, 212 (2015).

[13] A. K. Nayak, J. E. Fischer, Y. Sun, B. Yan, J. Karel, A. C. Komarek, C. Shekhar, N. Kumar, W. Schnelle, J. Kübler, and et al., Science Advances **2**, e1501870 (2016).

[14] N. Kiyohara, T. Tomita, and S. Nakatsuji, Physical Review Applied **5** (2016), 10.1103/physrevapplied.5.064009.

[15] T. Chen, T. Tomita, S. Minami, M. Fu, T. Koretsune, M. Kitatani, I. Muhammad, D. Nishio-Hamane, R. Ishii, F. Ishii, *et al.*, Nature Communications **12**, 1 (2021).

[16] M. Naka, S. Hayami, H. Kusunose, Y. Yanagi, Y. Motome, and H. Seo, Phys. Rev. B **102**, 075112 (2020).

[17] H. Tsai, T. Higo, K. Kondou, T. Nomoto, A. Sakai, A. Kobayashi, T. Nakano, K. Yakushiji, R. Arita, S. Miwa, *et al.*, Nature **580**, 608 (2020).

[18] L. Šmejkal, R. González-Hernández, T. Jungwirth, and J. Sinova, Science Advances **6** (2020), 10.1126/sciadv.aaz8809.

[19] Z. Feng, X. Zhou, L. Šmejkal, L. Wu, Z. Zhu, H. Guo, R. González-Hernández, X. Wang, H. Yan, P. Qin, *et al.*, arXiv preprint arXiv:2002.08712 (2020).

[20] F. D. M. Haldane, Phys. Rev. Lett. **61**, 2015 (1988).

[21] C.-Z. Chang, J. Zhang, X. Feng, J. Shen, Z. Zhang, M. Guo, K. Li, Y. Ou, P. Wei, L.-L. Wang, Z.-Q. Ji, Y. Feng, S. Ji, X. Chen, J. Jia, X. Dai, Z. Fang, S.-C. Zhang, K. He, Y. Wang, L. Lu, X.-C. Ma, and Q.-K. Xue, Science **340**, 167 (2013).

[22] R. Yu, W. Zhang, H.-J. Zhang, S.-C. Zhang, X. Dai, and Z. Fang, Science **329**, 61–64 (2010).

[23] I. Martin and C. D. Batista, Phys. Rev. Lett. **101**, 156402 (2008).

[24] J. W. F. Venderbos, M. Daghofer, J. van den Brink, and S. Kumar, Phys. Rev. Lett. **109**, 166405 (2012).

[25] H. Ishizuka and Y. Motome, Phys. Rev. B **87**, 081105 (2013).

[26] G.-W. Chern, A. Rahmani, I. Martin, and C. D. Batista, Phys. Rev. B **90**, 241102 (2014).

[27] P. B. Ndiaye, A. Abbout, V. M. L. D. P. Goli, and A. Manchon, Phys. Rev. B **100**, 144440 (2019).

[28] S. Eremeev, M. Otrokov, and E. Chulkov, Journal of Alloys and Compounds **709**, 172–178 (2017).

[29] J.-Q. Yan, Q. Zhang, T. Heitmann, Z. Huang, K. Y. Chen, J.-G. Cheng, W. Wu, D. Vaknin, B. C. Sales, and R. J. McQueeney, Phys. Rev. Materials **3**, 064202 (2019).

[30] B. Li, J.-Q. Yan, D. Pajerowski, E. Gordon, A.-M. Nedić, Y. Sizyuk, L. Ke, P. Orth, D. Vaknin, and R. McQueeney, Physical Review Letters **124** (2020), 10.1103/physrevlett.124.167204.

[31] A. Zeugner, F. Nietschke, A. U. B. Wolter, S. Gaß, R. C. Vidal, T. R. F. Peixoto, D. Pohl, C. Damm, A. Lubk, R. Hentrich, and et al., Chemistry of Materials **31**, 2795–2806 (2019).

[32] M. M. Otrokov, I. I. Klimovskikh, H. Bentmann, D. Estyunin, A. Zeugner, Z. S. Aliev, S. Gaß, A. U. B. Wolter, A. V. Koroleva, A. M. Shikin, and et al., Nature **576**, 416–422 (2019).

[33] C. Lei, S. Chen, and A. H. MacDonald, Proceedings of the National Academy of Sciences **117**, 27224–27230 (2020).

[34] M. M. Otrokov, T. V. Menshchikova, M. G. Vergniory, I. P. Rusinov, A. Yu Vyazovskaya, Y. M. Koroteev, G. Bihlmayer, A. Ernst, P. M. Echenique, A. Arnau, and et al., 2D Materials **4**, 025082 (2017).

[35] D. Zhang, M. Shi, T. Zhu, D. Xing, H. Zhang, and J. Wang, Phys. Rev. Lett. **122**, 206401 (2019).

[36] J. Li, Y. Li, S. Du, Z. Wang, B.-L. Gu, S.-C. Zhang, K. He, W. Duan, and Y. Xu, Science Advances **5**, eaaw5685 (2019).

[37] S. Chowdhury, K. F. Garrity, and F. Tavazza, npj Computational Materials **5** (2019), 10.1038/s41524-019-0168-1.

[38] D. S. Lee, T.-H. Kim, C.-H. Park, C.-Y. Chung, Y. S. Lim, W.-S. Seo, and H.-H. Park, CrystEngComm **15**, 5532 (2013).

[39] E. D. L. Rienks, S. Wimmer, J. Sánchez-Barriga, O. Caha, P. S. Mandal, J. Růžička, A. Ney, H. Steiner, V. V. Volobuev, H. Groiss, and et al., Nature **576**, 423–428 (2019).

[40] S. H. Lee, Y. Zhu, Y. Wang, L. Miao, T. Pillsbury, H. Yi, S. Kempinger, J. Hu, C. A. Heikes, P. Quarterman, W. Ratcliff, J. A. Borchers, H. Zhang, X. Ke, D. Graf, N. Alem, C.-Z. Chang, N. Samarth, and Z. Mao, Phys. Rev. Research **1**, 012011 (2019).

[41] M. M. Otrokov, I. P. Rusinov, M. Blanco-Rey, M. Hoffmann, A. Y. Vyazovskaya, S. V. Eremeev, A. Ernst, P. M. Echenique, A. Arnau, and E. V. Chulkov, Phys. Rev. Lett. **122**, 107202 (2019).

[42] C. Liu, Y. Wang, H. Li, Y. Wu, Y. Li, J. Li, K. He, Y. Xu, J. Zhang, and Y. Wang, Nature Materials **19**, 522–527 (2020).

[43] K. Y. Chen, B. S. Wang, J.-Q. Yan, D. S. Parker, J.-S. Zhou, Y. Uwatoko, and J.-G. Cheng, Phys. Rev. Materials **3**, 094201 (2019).

[44] Y. Deng, Y. Yu, M. Z. Shi, Z. Guo, Z. Xu, J. Wang, X. H. Chen, and Y. Zhang, Science **367**, 895–900 (2020).

[45] H. Deng, Z. Chen, A. Wołoś, M. Konczykowski, K. Sobczak, J. Sitnicka, I. V. Fedorchenko, J. Borysiuk, T. Heider, Ł. Pluciński, and et al., Nature Physics (2020), 10.1038/s41567-020-0998-2.

[46] Y. Gong, J. Guo, J. Li, K. Zhu, M. Liao, X. Liu, Q. Zhang, L. Gu, L. Tang, X. Feng, and et al., Chinese Physics Letters **36**, 076801 (2019).

[47] S. Zhang, R. Wang, X. Wang, B. Wei, B. Chen, H. Wang, G. Shi, F. Wang, B. Jia, Y. Ouyang, and et al., Nano Letters **20**, 709–714 (2019).

[48] H. Li, S.-Y. Gao, S.-F. Duan, Y.-F. Xu, K.-J. Zhu, S.-J. Tian, J.-C. Gao, W.-H. Fan, Z.-C. Rao, J.-R. Huang, J.-J. Li, D.-Y. Yan, Z.-T. Liu, W.-L. Liu, Y.-B. Huang, Y.-L. Li, Y. Liu, G.-B. Zhang, P. Zhang, T. Kondo, S. Shin, H.-C. Lei, Y.-G. Shi, W.-T. Zhang, H.-M. Weng, T. Qian, and H. Ding, Phys. Rev. X **9**, 041039 (2019).

[49] Y.-J. Hao, P. Liu, Y. Feng, X.-M. Ma, E. F. Schwier, M. Arita, S. Kumar, C. Hu, R. Lu, M. Zeng, Y. Wang, Z. Hao, H.-Y. Sun, K. Zhang, J. Mei, N. Ni, L. Wu, K. Shimada, C. Chen, Q. Liu, and C. Liu, Phys. Rev. X **9**, 041038 (2019).

[50] Y. J. Chen, L. X. Xu, J. H. Li, Y. W. Li, H. Y. Wang, C. F. Zhang, H. Li, Y. Wu, A. J. Liang, C. Chen, S. W. Jung, C. Cacho, Y. H. Mao, S. Liu, M. X. Wang, Y. F. Guo, Y. Xu, Z. K. Liu, L. X. Yang, and Y. L. Chen, Phys. Rev. X **9**, 041040 (2019).

[51] J. Ge, Y. Liu, J. Li, H. Li, T. Luo, Y. Wu, Y. Xu, and J. Wang, National Science Review **7**, 1280–1287 (2020).

[52] C. Hu, K. N. Gordon, P. Liu, J. Liu, X. Zhou, P. Hao, D. Narayan, E. Emmanouilidou, H. Sun, Y. Liu, and et al., Nature Communications **11**, 1 (2020).

[53] L. Ding, C. Hu, F. Ye, E. Feng, N. Ni, and H. Cao, Phys. Rev. B **101**, 020412 (2020).

[54] P. Swatek, Y. Wu, L.-L. Wang, K. Lee, B. Schrunk, J. Yan, and A. Kaminski, Phys. Rev. B **101**, 161109 (2020).

[55] S. V. Eremeev, M. M. Otrokov, and E. V. Chulkov, Nano letters **18**, 6521 (2018).

[56] J. Wu, F. Liu, M. Sasase, K. Ienaga, Y. Obata, R. Yukawa, K. Horiba, H. Kumigashira, S. Okuma, T. Inoshita, and et al., Science Advances **5**, eaax9989 (2019).

[57] R. C. Vidal, A. Zeugner, J. I. Facio, R. Ray, M. H. Haghighi, A. U. B. Wolter, L. T. Corredor Bohorquez, F. Caglieris, S. Moser, T. Figgemeier, T. R. F. Peixoto, H. B. Vasili, M. Valvidares, S. Jung, C. Cacho, A. Alfonsov, K. Mehlawat, V. Kataev, C. Hess, M. Richter, B. Büchner, J. van den Brink, M. Ruck, F. Reinert, H. Bentmann, and A. Isaeva, Phys. Rev. X **9**, 041065 (2019).

[58] I. I. Klimovskikh, M. M. Otrokov, D. Estyunin, S. V. Eremeev, S. O. Filnov, A. Koroleva, E. Shevchenko, V. Voroshnin, A. G. Rybkin, I. P. Rusinov, *et al.*, npj Quantum Materials **5**, 1 (2020).

[59] H. Sun, B. Xia, Z. Chen, Y. Zhang, P. Liu, Q. Yao, H. Tang, Y. Zhao, H. Xu, and Q. Liu, Phys. Rev. Lett. **123**, 096401 (2019).

[60] M. Gu, J. Li, H. Sun, Y. Zhao, C. Liu, J. Liu, and Q. Liu, "Surface anomalous hall effect and its quantization in magnetic topological crystals," (2020), arXiv:2005.13943 [cond-mat.mes-hall].

[61] S. Wimmer, J. Sánchez-Barriga, P. Küppers, A. Ney, E. Schierle, F. Freyse, O. Caha, J. Michalicka, M. Liebmann, D. Primetzhofer, M. Hoffmann, A. Ernst, M. M. Otrokov, G. Bihlmayer, E. Weschke, B. Lake, E. V. Chulkov, M. Morgenstern, G. Bauer, G. Springholz, and O. Rader, "Ferromagnetic mnsb2te4: A topological insulator with magnetic gap closing at high curie temperatures of 45-50 k," (2020), arXiv:2011.07052 [cond-mat.mtrl-sci].

[62] I. Belopolski, S.-Y. Xu, N. Koirala, C. Liu, G. Bian, V. N. Strocov, G. Chang, M. Neupane, N. Alidoust, D. Sanchez, H. Zheng, M. Brahlek, V. Rogalev, T. Kim, N. C. Plumb, C. Chen, F. Bertran, P. Le Fèvre, A. Taleb-Ibrahimi, M.-C. Asensio, M. Shi, H. Lin, M. Hoesch, S. Oh, and M. Z. Hasan, Science Advances **3** (2017), 10.1126/sciadv.1501692.

[63] See Supplemental Material for more information.

[64] C. Lei, O. Heinonen, A. H. MacDonald, and R. J. McQueeney, Phys. Rev. Materials **5**, 064201 (2021).

[65] C. Lei and A. H. MacDonald, Phys. Rev. Materials **5**, L051201 (2021).